4

Structure, Morphology, and Stoichiometry of GaN(0001) Surfaces Through Various Cleaning Procedures

Azusa N. Hattori[1] and Katsuyoshi Endo[2]
[1]*Nanoscience and Nanotechnology Center, The Institute of Scientific and Industrial Research, Osaka University*
[2]*Research Center for Ultra-Precision Science and Technology, Graduate School of Engineering, Osaka University*
Japan

1. Introduction

Perfect surfaces are expected to upgrade the quality of films grown on them. Generally, the surface plays a crucial role for a thin-film system, because of the large contribution of the interface and surface regions. The structures of clean surfaces are of particular importance since knowledge of the structures is the first step in understanding the fundamental issues of contact formation, chemical reactivity, growth processes, and so on.

Gallium nitride (GaN) has excellent properties such as a direct and wide band-gap energy, and high electron mobility, and has thus attracted much attention owing to its application in a wide range of electronic devices. For practical device fabrication, various materials have been integrated on GaN substrate surfaces, where the initial GaN surfaces often play a crucial role in the device operation. A number of groups have investigated GaN cleaning procedures for device fabrication. However, there is no standard method of preparing GaN substrates using chemical solutions or by ultra high-vacuum (UHV) treatment, and the results obtained in previous studies were not in conformity with one another. Through the various processes of cleaning GaN(0001) surfaces, we found a strong interrelation between surface morphology and stoichiometry; rough surfaces have broken stoichiometry while flat surfaces retain their stoichiometry (Hattori et al., 2009; 2010).

In this chapter we summarize the surface structures, morphology, and stoichiometry of GaN surfaces treated by annealing in UHV, sputtering, and chemical solutions. For the UHV-treated GaN surfaces, there were structure differences among samples subjected to the same treatment, and we clarify the effect of crystal quality, such as dislocations, the concentration of hydrogen impurities, and the residual reactant molecules in GaN films, on the surface structure. In the case of performing wet etching on a GaN system, selecting an etchant solution with a certain pH and oxide-reduction potential and controlling the etching time are important to obtain an oxide-free and balanced-stoichiometry surface. Finally, the reactions of GaN in solutions will be explained on the basis of the theoretical potential-pH

equilibrium diagram. At first, the backgrounds of GaN crystal, and GaN(0001) surface structures are introduced in section 2 and 3, respectively. Surface structure, morphology, and stoichiometry through each treatment are reported in section 4. Two different hydride vapor phase epitaxy (HVPE) freestanding GaN(0001) single crystal substrates were prepared; HVPE1 and HVPE2 which were purchased from different suppliers. The details of experimental condition and all references were written in Ref.(Hattori et al., 2009; 2010).

2. GaN crystal

GaN has excellent properties such as a direct and wide band-gap energy of 3.4 eV at room temperature (RT). It also has high electron mobility, and has thus attracted much attention for its potential use in a wide range of electronic devices. Usually GaN crystal (Fig. 1) has a hexagonal phase (wurtzite, a = 0.319 nm and c = 0.519 nm) (Edgar, 1994; Strite & Morkoc, 1992).

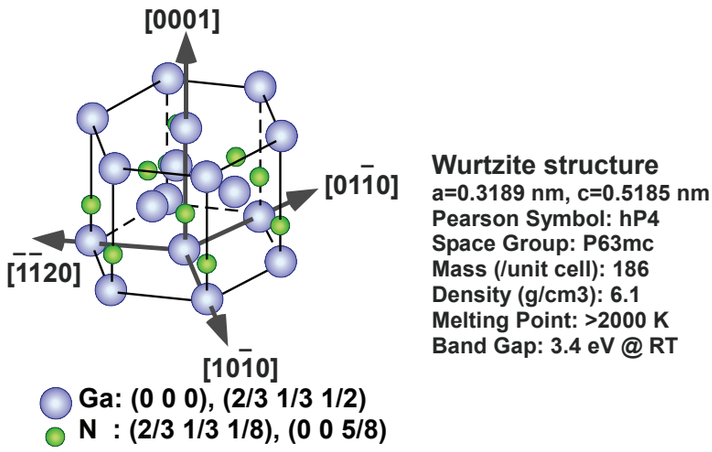

Fig. 1. Crystal structure of wurtzite GaN.

Figure 2 shows the atomic structures of each GaN face. The most common face of GaN is Ga-polar GaN(0001) (c-face), and recently non polar $(11\bar{2}0)$ (a-face) and $(10\bar{1}0)$ (m-face) GaN have been used for applications. The c-axis-oriented optoelectronic devices in particular suffer from undesirable spontaneous and piezoelectric polarization effects. The aim to eliminate such detrimental effects has led to renewed interest in non polar (a- and m-plane) GaN (Waltereit et al., 2000).

2.1 HVPE

For commercially available samples, the major fabrication method is hydride vapor phase epitaxy (HVPE). In the HVPE method, GaCl and NH_3 react to produce GaN, with H_2 and HCl gases as by-products: $GaCl + NH_3 \rightarrow GaN + H_2 + HCl$ (Maruska & Tietjen, 1969) (Fig. 3).

The crystallinity (such as defect density) and/or properties of GaN strongly depend on the growth conditions. HVPE GaN has a threading dislocation density of about 10^6-10^7 cm^{-2}, although GaN crystal quality has been improved in recent years and is expected to be improved, further. HVPE growth (Maruska & Tietjen, 1969) is a very popular method of fabricating both crystalline substrates and homoepitaxial layers because of the high

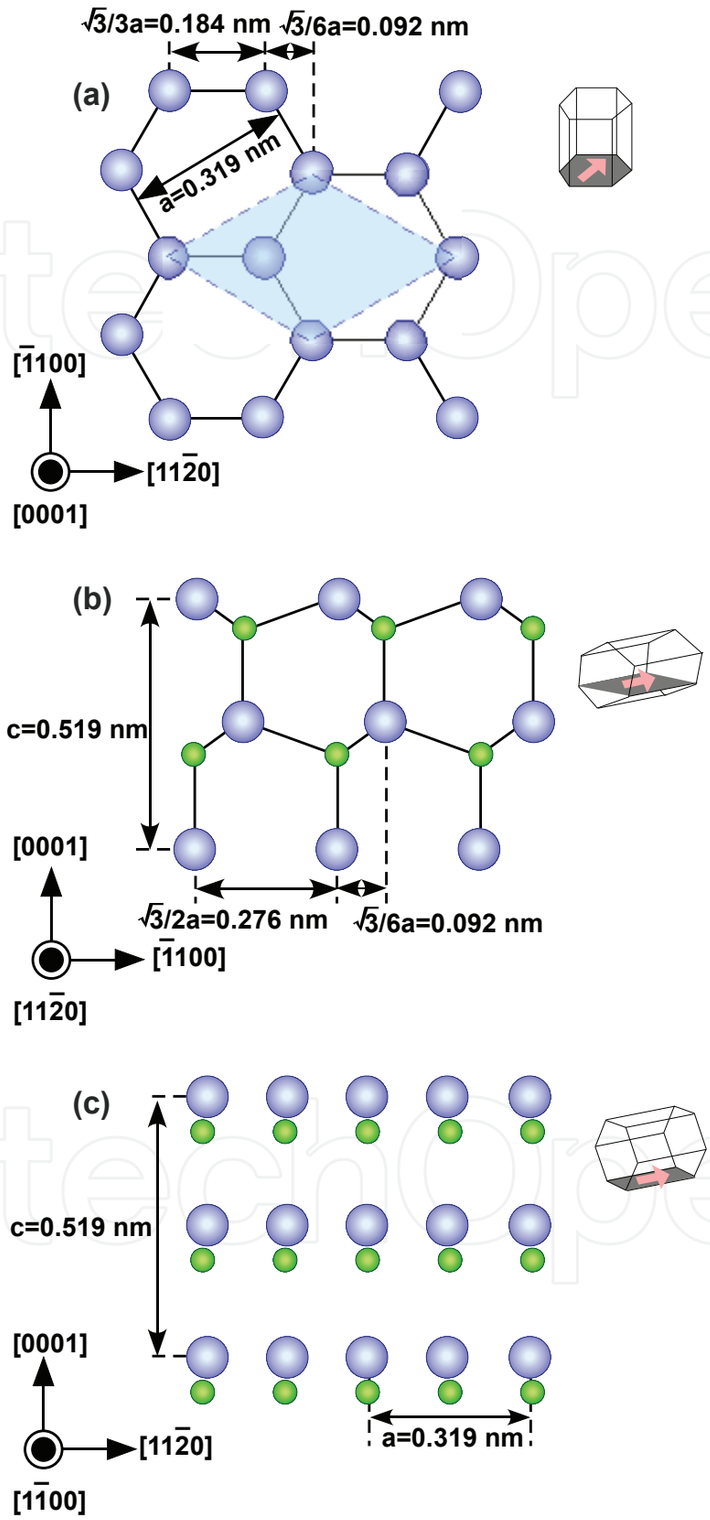

Fig. 2. Atomic arrangement of (a) GaN(0001) (*c*-face), (b) GaN(11$\bar{2}$0) (*a*-face), and (c)(10$\bar{1}$0) (*m*-face). The atomic arrangement is shown in the direction of each arrow in the inset crystals.

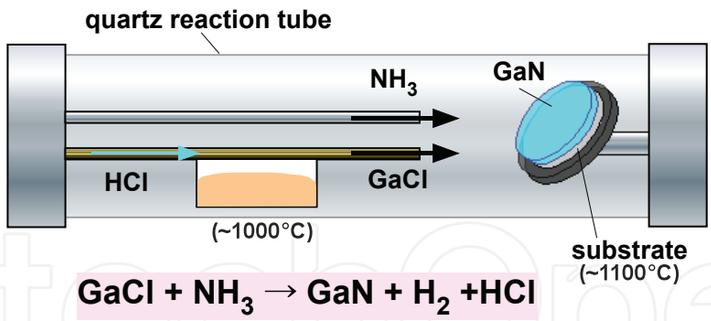

Fig. 3. Schematic illustration of HVPE growth method. The growth is performed in a quartz tube reactor by bubbling a hydrogen chloride (HCl) gas flow over a Ga melt, which results in the formation of gaseous gallium chloride (GaCl). The GaCl flows through the nozzle towards the sample, where it reacts with ammonia (NH_3) to form GaN.

growth rates of around 100 μm/hr. Also, many methods of stably fabricating larger and higher-quality GaN crystals at a low price by HVPE growth have been patented. Of course, dislocations severely influence device performance, though GaN crystals have been realized as products in the laser market. To achieve electronic devices with excellent properties, for instance, carrier transport, we should improve the crystal quality and surface-finishing methods and understand the local (microscopic) surface structure that becomes the interface under electrode materials. A dislocation density of less than 10^3 cm^{-2} is required for laser diode applications to obtain a higher yield and cost-effectiveness. Many researchers have tried to fabricate GaN crystals with lower dislocation densities.

2.2 Hydrogen impurity

The crystal properties and surface structures of GaN are affected by impurities in the crystals; in particular, the presence of hydrogen as an impurity has been reported (Nickel, 1999). It was shown that H in GaN exhibits unique features which have not been observed in more traditional semiconductors such as Si and GaAs (Nickel, 1999), for example, the formation of an acceptor-hydrogen complex, especially in GaN:Mg, with p-type conductivity. Also, the presence of ambient H changes the formation energy of the GaN surface and causes the formation of reconstruction structures. The hydrogen impurity sometimes arises from an impurity component of the source gases, especially ammonia. A hydrogen concentration of 10^{19}-10^{23} cm^{-3} was measured for molecular beam epitaxy (MBE)-GaN by nuclear reaction analysis, and a strong correlation between hydrogen concentration and crystal strain (dislocations) was observed. This correlation leads to a higher density of the hydrogen impurity in metal-organic chemical vapor deposition (MOCVD) films than in HVPE substrates (Hattori et al., 2009), affecting the dislocation density, when the hydrogen impurity is supplied from the source gases.

Figure 4(a) shows the typical major temperature programmed desorption (TPD) curves of an as-received HVPE1 sample. The temperature was ramped up at a rate of 0.5 K/s. Similar TPD curves to those in Fig. 4(a) were observed for the HVPE2 sample. As shown in the figure, the major detected values of m/e are 2, 12, 14, 16, 17, 18, 28, 35, 36, 69, and 104 in atomic units (AMU), which can be assigned to H_2^+, C^+, N^+/CH_2^+, O^+/NH_2^+, OH^+/NH_3^+, H_2O^+,

N_2^+/CO^+, Cl^+, HCl^+, Ga^+, and $GaCl^+$, respectively. Thus, the main desorption species are considered to be H_2, CH_4, NH_3, H_2O, N_2, CO, (H)Cl, Ga, and GaCl.

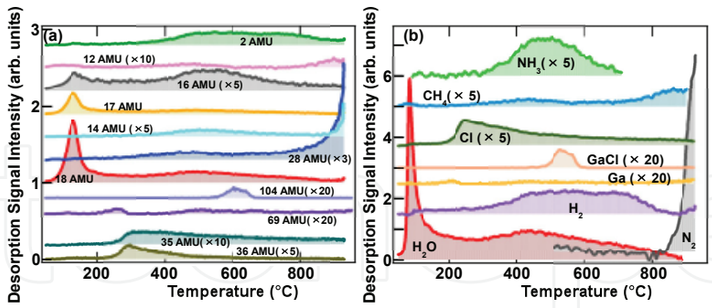

Fig. 4. (a) TPD curves of major mass numbers detected for HVPE1 samples. (b) TPD spectra of desorption species estimated from (a) considering the cracking elements and ratio. The temperature was ramped up at a rate of 0.5 K/s. The TPD curves for HVPE2 samples were similar to those for HVPE1 samples.

Figure 4(b) shows the desorption curves of these species estimated from Fig. 4(a). H_2O peaks below 200°C, N_2 peaks above 800°C, and broad H_2 peaks from 400 to 800°C can be seen for both samples. The origin of the H_2O desorption should be physical adsorption on the surface from humidity in the air. The m/e = 35 (Cl^+), 36 (HCl^+), and 104 ($GaCl^+$) peaks were clearly observed. In the HVPE method (Fig. 3), GaCl and NH_3 react to produce GaN, with H_2 and HCl gases as by-products: $GaCl + NH_3 \rightarrow GaN + H_2 + HCl$ (Maruska & Tietjen, 1969). The desorption of GaCl, (H)Cl, NH_3, and H_2 in HVPE-GaN samples strongly indicates that they originated from unreacted source materials and/or residual product materials. This implies that the HVPE growth conditions are not yet optimized. In the TPD of MOCVD samples, no GaCl desorption and little Cl desorption were detected (Hattori et al., 2009). In the MOCVD process, the gallium and nitrogen sources are usually $Ga(CH_3)_3$ and NH_3, respectively, and the products are GaN and CH_4: $Ga(CH_3)_3 + NH_3 \rightarrow GaN + 3CH_4$ (Amano et al., 1986). It was reported that intense CH_4 desorption occurs from MOCVD samples rather than HVPE samples (Hattori et al., 2009); the CH_4 species is one of the by-product elements in the MOCVD film and/or from surface carbon contamination.

3. GaN(0001) surface structures

3.1 GaN(0001)2×2 surface structures

The structures of clean surfaces are of particular importance since knowledge of the structures is the first step in understanding the fundamental issues of contact formation, chemical reactivity, growth processes, and so on. The surface structures of as-grown samples of Ga-polar GaN(0001) grown by MBE and MOCVD on substrates of Si-polar SiC(0001), sapphire(0001), Si(111), and so on have been studied *in-situ*. For the MBE growth of a GaN(0001) surface under a Ga-rich condition, 2×2, 2×3, 3×2, 3×4, 4×4, 5×5, 10×10, $5\sqrt{3}\times2\sqrt{13}$, 5×2.5, $\sqrt{7}\times\sqrt{7}$, and $\sqrt{3}\times\sqrt{3}$ reconstruction structures have been reported. In general, the unintentional presence of arsenic on the surface leads to these MBE reconstruction structures.

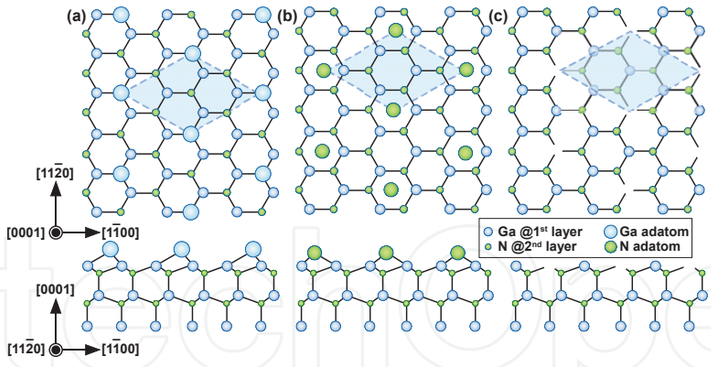

Fig. 5. GaN(0001)2×2 models: (a) Ga adatom, (b) N adatom, and (c) vacancy.

Ordered 1×1 and 2×2 reconstruction structures are formed on GaN(0001) surfaces. On samples grown by MOCVD, an ordered 1×1 surface with a nearly one-to-one stoichiometric composition has been reported. Figure 5 shows the 2×2 reconstruction models. Some theoretical studies have predicted that a GaN(0001) surface exhibits a 2×2 reconstruction structure under a Ga-rich condition: GaN(0001)2×2-Ga and its minimum-energy configuration have been proposed. Reconstructed GaN(0001)2×2 surfaces (GaN(0001)2×2-N), however, have been reported as a result of experiments on samples grown by MBE under nitrogen-rich growth conditions. These studies were performed *in-situ*; films were fabricated by controlling the stoichiometry in UHV, where the surfaces were subsequently observed. These *in-situ* methods cannot be universally applied to commercial sample surfaces.

3.2 As-received HVPE-GaN(0001) surface structures

Figure 6 shows low-energy electron diffraction (LEED) and reflection high-energy electron diffraction (RHEED) patterns of the two different as-received commercial HVPE1 and HVPE2 samples. LEED patterns of the HVPE1 sample (Fig. 6(a)) and HVPE2 sample (Fig. 6(b)) show almost no specific features. Note that LEED in this E_p range reflects the ordering of a few surface layers. It was reported that an MOCVD-grown GaN(0001) surface is terminated by hydrogen, and that MOCVD-grown GaN(0001) show clear 1×1 spots even after exposure to air (Hattori et al., 2009). That is why the survival of the 1×1 ordering on MOCVD samples is caused by an inert H-termination cap, similar to the case of Si(001)-H surfaces.

In general, commercially available GaN sample surfaces are surface-lapped (mechanically polished) and finished by chemical mechanical polishing (CMP), dry etching, and so on, after fabrication and subsequent exposure to air. The surface figuring treatments are performed to obtain mirror-polished smooth surfaces, where the presence of a surface oxide layer was reported. Thus, no specific LEED spots indicates that surface crystallinity and ordering were clearly destroyed in at least a few surface layers by the surface-finishing treatments.

In the RHEED patterns for the HVPE1 (Fig. 6(c)) and HVPE2 (Fig. 6(d)) samples, where the electron mean free path at this E_p is ∼20 nm (Ichimiya & Cohen, 2004), we observed weak transmission diffraction spots (cyan circles) in addition to clear 1×1 surface spots (dashed arcs, corresponding to Laue zones). The transmission spots indicate the existence of 3D islands of

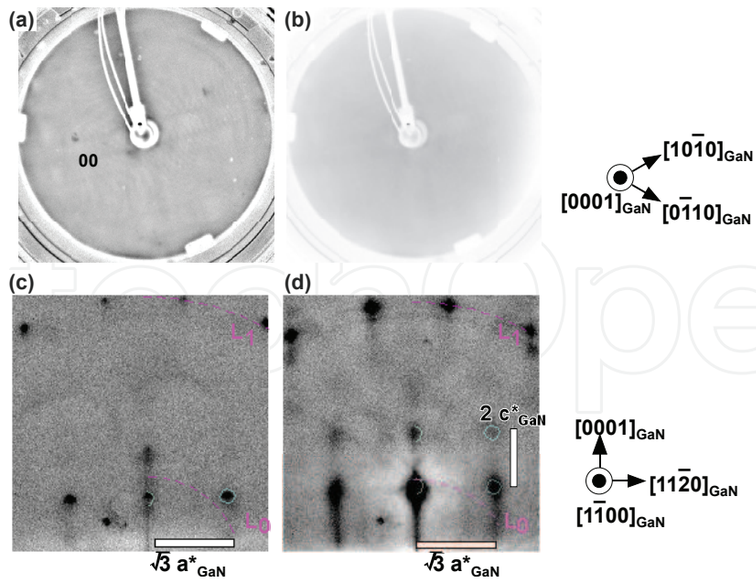

Fig. 6. LEED and RHEED patterns of as-received samples: (a) and (c) HVPE1, and (b) and (d) HVPE2 samples, respectively. Note that the 00 beam in LEED was not at the screen center. The incident electron direction was $[1\bar{1}00]$ in RHEED. E_p in LEED was 95 eV. In RHEED, Laue zones (L_0 and L_1) and transmission spots are indicated by pink dashed arcs and cyan circles, respectively. The scales of a^* and c^* are the reciprocal lattice units corresponding to a and c, respectively.

GaN(0001) on the as-received GaN(0001) surfaces. The main purpose of the surface-finishing treatments is to remove damage by lapping and to achieve surface flattening without damage. However, no effective polishing method or etchant has yet been confirmed for GaN substrates, although macroscopic surface roughness has been improved. Murata *et al.* evaluated the thickness of damage (depth profile) in commercial HVPE GaN substrates treated by CMP by measuring photocurrent density. They concluded that commercial HVPE GaN substrates have a damaged layer with a thickness of a few hundred nm and many scratches on the surface (Murata et al., 2009).

Figures 7(a) and (b) show the core-level spectra of Ga $3d_{5/2,3/2}$ and N 1s, respectively, for the as-received HVPE1 sample obtained by X-ray photoelectron spectroscopy (XPS). The Ga 3d spectra are asymmetric and can be fitted with four symmetric Voigt components with different chemical shifts corresponding to Ga bonding to nitrogen: Ga_N (binding energy (BE) = 19.2-20.3 eV), Ga bonding to oxygen: Ga_{O_x} (BE = 19.6-21.0 eV), Ga bonding to N-H: Ga_{H-N} (BE = 19.21 eV), and metal-Ga (BE = 18.4-18.49 eV). It is known that hydrogen is unintentionally doped in GaN, and hydrogen behavior in GaN films has been investigated by Fourier transform infrared (FTIR) absorption, electron-energy-loss spectroscopy, and so on. Kong *et al.* confirmed the stretch mode of the N-H bond by FTIR and denoted the hydrogen-related complex as Ga$\cdots$H-N. They also assigned a Ga$\cdots$H-N peak in the Ga 3d spectra in XPS. Note that the energy difference between Ga $3d_{3/2}$ and Ga $3d_{5/2}$ is less than 0.1 eV, negligible compared with our resolution. Upon comparing GaN samples with and without CMP treatment after film fabrication, we found a small Ga_{O_x} peak and negligible

metal-Ga peaks in the no-CMP samples (Hattori et al., 2009). For the enhancement of the GaO_x and metal-Ga peaks in the as-received HVPE1 sample, we consider that CMP treatment after film(crystal) fabrication destroys the surface termination, promotes oxidation, and induces the formation of Ga metal impurities and/or segregation. The surface oxidation and the existence of metal impurities after CMP have been pointed out to be general phenomena. These results also indicate that CMP treatment has a severe effect on the surface structures and condition. Note that the existence of Ga oxide layers with a thickness of ~ 1.5 nm was reported for HPVE samples.

The N 1s spectra can be fitted with five components: N 1s core electrons bonding to hydrogen: N_{H_3} (BE = 405.6-406.2 eV) and N_{H_2} (BE = 397.7-399.72 eV), an N 1s core-electron bonding to gallium: N_{Ga} (BE = 396.2-397.86 eV), and two Ga LMM Auger electrons with satellites. There is no significant difference of the N 1s spectra between the HVPE and MOCVD samples. The impurity components of O 1s, C 1s, and Cl 2p were observed by XPS. From the intensities of these components, we can estimate their atomic percentages (atomic%) in the surface region using the established photoelectron cross sections and mean free paths. Table 1 summarizes the atomic% of each component for the HVPE1 and HVPE2 samples. Here, the sum of Ga, N, O, C, and Cl atomic% is fixed to 100%. We can confirm that the as-received HVPE1 and HVPE2 samples include non-negligible amounts of O, C, and Cl as impurities.

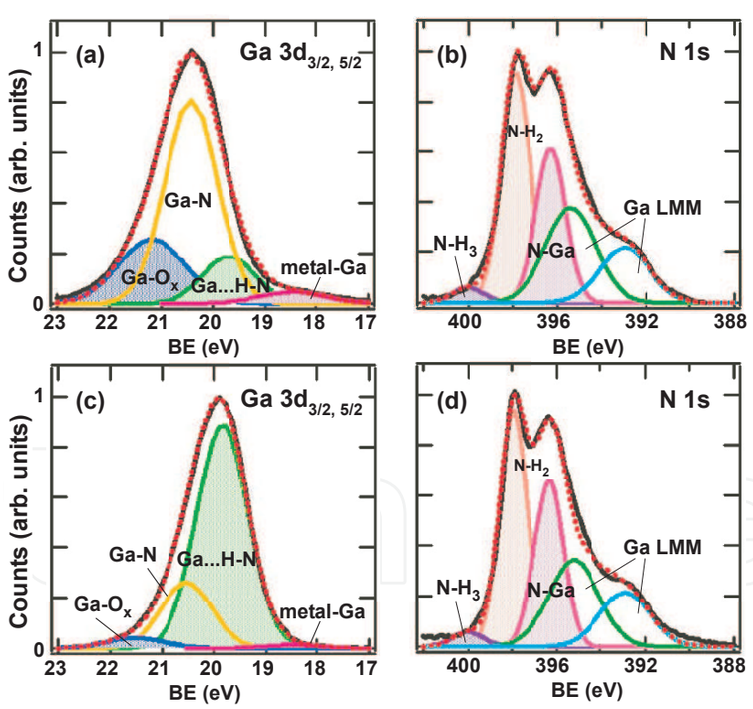

Fig. 7. Core-level XPS spectra of (a) and (c) gallium 3d, and (b) and (d) nitrogen 1s: (a) and (b) for an as-received (non etched) HVPE1 sample, and (c) and (d) for a 100 s HF-etched HVPE1 sample. Measured Ga 3d and N 1s spectra (black curves) are fitted with Voigt functions of four components (Ga_N, Ga_{O_x}, Ga_{H-N}, and metal-Ga) and five components (N_{Ga}, N_{H_2}, N_{H_3}, and two Ga LMM Auger satellites), respectively. The red dashed curves indicate the sum of the component peaks.

4. Surface stoichiometry through treatments

4.1 Annealing in UHV

Figure 8 shows schematic phase diagrams of (a) HVPE substrates (HVPE1 and HVPE2) after annealing, determined by LEED, RHEED, XPS, Auger electron spectroscopy (AES), TPD, and scanning tunneling microscope (STM) measurements. Relatively clean surfaces were obtained by annealing the HVPE samples; 1×1 structures exist on the HVPE surfaces after annealing at approximately 500-600°C. At a higher annealing temperature (≥500-600°C), nitrogen sublimation in the form of ammonia started to occur and 3D islands with facets formed. Finally, samples were damaged after annealing above 800°C.

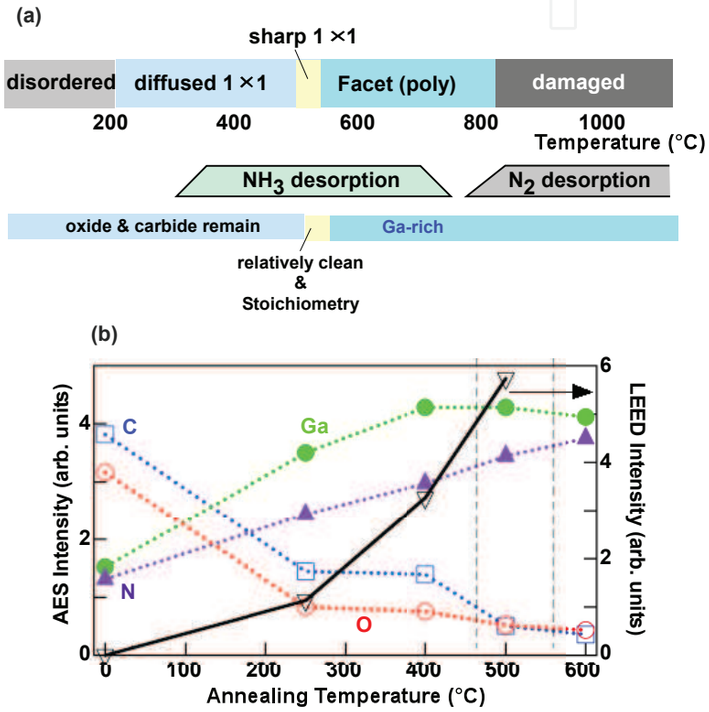

Fig. 8. Schematic phase diagrams for HVPE1 and HVPE2 samples treated by annealing in UHV. Nitrogen sublimates in two forms: as ammonia at around 300-700°C and as molecular nitrogen above 800°C. The phases were observed at RT after annealing. (b) Intensity change of (10) LEED spots as a function of annealing temperature (open black inverted triangles). In addition, the AES intensities of C (277 eV, open blue squares), N (392 eV, filled violet triangles), O (525 eV, open red circles), and Ga (1098 eV, filled green circles) are plotted against annealing temperature. In (b) annealing was performed at 250°C for 12 hrs., 400°C for 1 hr, 500°C for 10 min, and 600°C for 10 min. The incident E_p for LEED and AES were 95 eV and 2 keV, respectively.

We found that three-step annealing results in relatively clean and flat surfaces with balanced stoichiometry. The established conditions for each step were (1) 200°C for 12 hrs., (2) 400°C for 1 hr, and (3) 500°C for 5 min. AES signals (Fig. 8(b)) showed the reduction of oxide and carbide from the surface upon annealing at ~200 and 500°C, which is consistent with the TPD results (Fig. 4). Figure 9(a) shows an LEED pattern and a typical STM image of an HVPE1 sample

annealed (degassed) at 200°C for 12 hrs. The LEED pattern showed a diffused 1×1 structure and STM indicated that many clusters remained on the surface. These clusters are ascribed to the formation of oxide/carbide layers. The peak-to-valley (PV) height and root-mean-square (RMS) roughness were 2.5 and 0.86 nm, respectively. After another two steps, the sharpest 1×1 LEED patterns appeared and STM images showed wide and flat terraces of ∼10 nm size and steps, as shown in Fig. 9(b). PV and RMS were 1.7 and 0.39 nm, respectively. Sharp 1×1 spots without any transmission spots are seen in the RHEED pattern, as shown in Fig. 9(c). On relatively clean surfaces, the AES intensities of C and O decreased to ∼20% of those for the as-received surfaces, but no ordered atomic arrangements were observed anywhere.

Table 1. Atomic percentages of surface species, Ga, N, O, C, and Cl for HVPE1 and HVPE2 samples with different treatments (as-received, 600°C annealing in UHV, Ar^+ sputtering, and 100 sec-HF, 500 sec-HF, and 700 sec-HNO_3 etching), determined by XPS intensities and sensitivity factors for Ga 3d, N 1s, O 1s, C 1s, and Cl 2p. As shown in Figs. 2, we can estimate the component intensities of Ga_N, Ga_{O_x}, Ga_{H-N}, and metal-Ga from Ga 3d spectra, and those of N_{Ga}, N_{H_2}, and N_{H_3} from N 1s spectra. Here the sum of Ga, N, O, C, and Cl atomic-% is fixed to be 100%. Note that these values have an error of approximately ±10%, e.g., 16% is 16±2%.

Sample	Treatment	Ga [%]					N [%]				O	C	Cl
		Ga_N	Ga_{H-N}	Ga_{O_x}	metal	sum	N_{Ga}	N_{H_2}	N_{H_3}	sum	[%]	[%]	[%]
HVPE1	received	16	9	13	2	**40**	15	22	6	**43**	**6**	**11**	**<1**
	sputtering	26	20	–	–	**46**	22	25	4	**51**	**2**	**–**	**<1**
	annealing	18	15	8	1	**42**	21	14	3	**38**	**11**	**8**	**<1**
	100 sec-HF	9	30	2	<1	**41**	19	26	2	**47**	**3**	**9**	**<1**
	500 sec-HF	7	26	2	<1	**35**	24	26	5	**55**	**3**	**7**	**<1**
	700 sec-HNO_3	8	27	2	<1	**37**	24	26	2	**52**	**3**	**8**	**<1**
HVPE2	received	13	19	3	2	**37**	20	20	3	**43**	**11**	**8**	**<1**

In the HVPE2 samples, similar dependence of the behavior of surface structures on the annealing temperature to that shown in the HVPE1 sample was confirmed. However, the microscopic structures observed by STM were quite different from those of the HVPE1 sample. Figure 10 shows an RHEED pattern and typical STM image of an HVPE2 sample after three-step annealing (200°C for 12 hrs. + 400°C for 1 hr. + 500°C for 5 min). Sharp 1×1 spots without any transmission spots are seen in the RHEED pattern, as shown in Fig. 10(a). The LEED pattern also showed sharp 1×1 spots. The STM image indicated a flat surface with numerous grains of a few nm in size as shown in Fig. 10(b). Some grains gathered to form petal-like shapes (indicated by a diamond in the inset in Fig. 10(b)). On less than a few percent of the surface area, the petal-like structures coalesced with each other (indicated by diamonds in Fig. 10(c)), but these structures are scattered. The side length of the diamonds is ∼2 nm; thus, the area of one petal-like structure corresponds to $\approx 6a \times 6a$. Note that the directions of the sides of the diamonds are parallel to the $\langle 11\bar{2}0 \rangle$ directions. These petal-like structures resemble those in the STM image in Ref. (Feenstra et al., 2000), where a 12×12-reconstructed structure, which had not been previously observed on (0001) or (000$\bar{1}$) surfaces. Feenstra *et al.* (Feenstra et al., 2000) associated this novel structure with the "1×1" Ga adlayers on GaN(0001) layers, implying the existence of an inversion domain immediately below the novel reconstruction area of the surface. On HVPE2 sample surfaces, petal-like structures were reproducibly observed but neither pits nor holes were observed. They were present in at

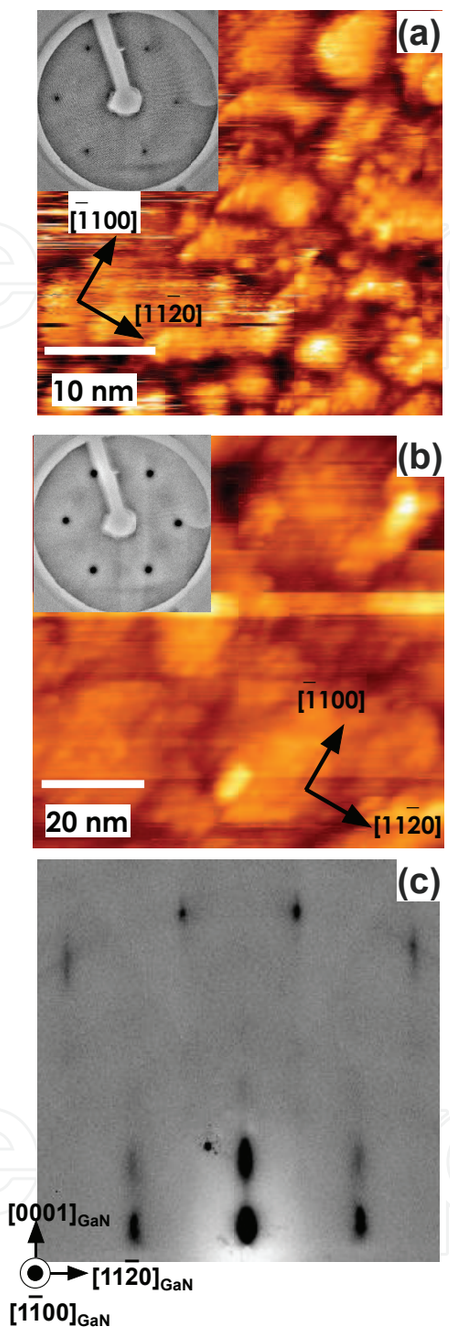

Fig. 9. (a) Typical STM image and LEED pattern after degassing at 200°C for 12 hrs. (b) Typical STM images and LEED pattern (in inset), and (c) RHEED pattern after three-step annealing (200°C for 12 hrs., 400°C for 1 hr, and 500°C for 10 min). The observed conditions were (a) $E_p = 85$ eV, $V_s = -4.8$ V, $I_t = 0.3$ nA; (b) $E_p = 85$ eV, $V_s = -5.0$ V, $I_t = 0.1$ nA; and (c) $[1\bar{1}00]$ incident, 15 kV.

most a few % in the whole observed area. The HVPE2 sample was grown by multistep lateral epitaxial overgrowth, and there are defects distributed inside this crystal. Thus, we associate the petal-like structure on the surface with an area with high defect density immediately below the inside of the crystal, and conclude that the petal-like structure in this study is correlated with the novel reconstruction in the prior work (Feenstra et al., 2000). The petal-like structures observed on HVPE2 samples were not observed on HVPE1 samples.

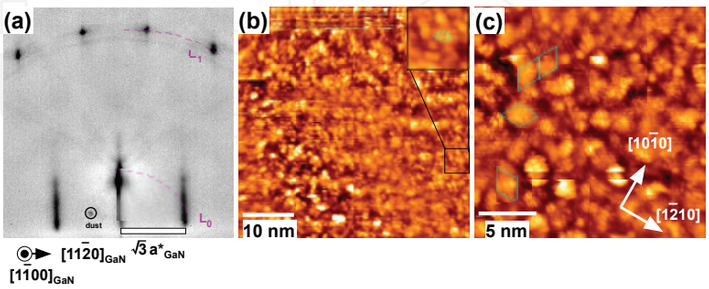

Fig. 10. (a) Typical STM image and LEED pattern (inset) after degassing at 200°C for 12 hrs. (b) Cross-sectional profile through the dashed line in (a); PV and RMS were 2.5 and 0.86 nm, respectively. (c) and (e) Typical STM images and LEED pattern (in inset of (c)) after three-step annealing (200°C for 12 hrs., 400°C for 1 hr, and 500°C for 10 min). (d) and (f) Cross-sectional profiles through the dashed lines in (c) and (e), respectively. PV and RMS in (d) were 1.7 and 0.39 nm, respectively. The observed conditions were (a) $E_p = 85$ eV, $V_s = -4.8$ V, $I_t = 0.3$ nA; (c) $E_p = 85$ eV, $V_s = -5.0$ V, $I_t = 0.1$ nA; and (e) $V_s = +4.2$ V, I_t = 0.5 nA.

Annealing in UHV, which is one of the general methods of obtaining clean and well-defined surfaces, could not produce the expected clean GaN surfaces; only postannealing below ∼550°C could reduce (but not eliminate) surface contamination while maintaining the stoichiometry; however, it did not induce any surface reconstructions. The annealing treatment at high temperature removed surface contamination completely, but facets started to appear on the GaN surface above 550°C and the surface become Ga-rich with unbalanced stoichiometry (Table 1).

Figure 11(a) shows a typical RHEED pattern of a HVPE1 sample annealed at 600°C for 20 min after the three-step annealing. We can see characteristic "chevrons" in the RHEED patterns, corresponding to facets, in addition to transmission spots from 3D GaN islands. The transmission spot intensities were weak, indicating a small number of epitaxial islands. The chevron patterns were broad, indicating small domains. Although the chevron directions are $\langle 11\bar{2}4\rangle$ at the $[1\bar{1}00]$ incidence (Fig. 6(a)), we consider that these are part of $\langle 101\bar{2}\rangle$ reciprocal rods, which correspond to $\{101\bar{2}\}$ facets, from the LEED results of Fig. 11(b). Figures 11(b) and (c) respectively show an LEED pattern and a typical STM image of a HVPE1 sample annealed at 600°C for 5 min after the three-step annealing. We can see characteristic spots in the LEED pattern (some of them are indicated by arrows); the motion of these spots with changing E_p was different from that of the fundamental spots, reflecting the inclined reciprocal rods of the facets. The motion of the facet spots was restricted in the directions from the 00 spots to the 10, 01, $\bar{1}1$, $\bar{1}0$, $0\bar{1}$, and $1\bar{1}$ spots, implying that the inclined reciprocal rods are oriented in the $\langle 10\bar{1}n\rangle$ directions. Since the projection of the RHEED chevrons with the $\langle 11\bar{2}4\rangle$ direction (Fig. 11(a)) in the $\langle 10\bar{1}n\rangle$ direction gives the $\langle 10\bar{1}2\rangle$ direction, we consider the existence of six

fold facets of $\{10\bar{1}2\}$. This facet plane is the so-called R-plane. There have been many reports about facets formed on GaN surfaces. Most of them were formed during chemical etching and at the beginning of crystal fabrication, where facets with a size of few tens of μm, for example, $\{10\bar{1}\bar{1}\}$ facets, were formed. The $\{10\bar{1}\bar{2}\}$ orientation of the facet planes on GaN(0001) films has also been reported. For MOCVD GaN(0001) samples annealed at around 800-900°C in UHV, facet LEED patterns were reported in some references.

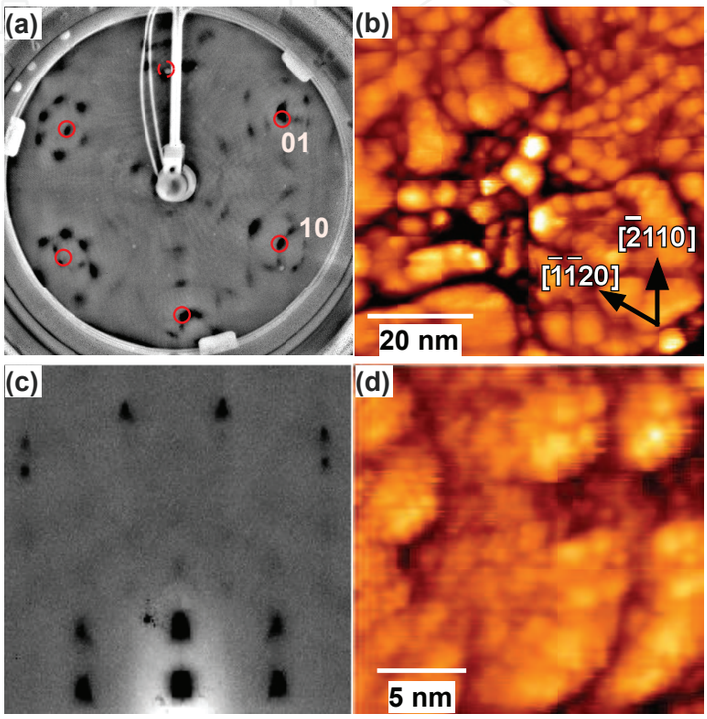

Fig. 11. (a) LEED pattern (E_p = 68 eV) of HVPE1 sample annealed at 600°C for 5 min after three-step annealing. Fundamental spots are marked by red circles. The other spots correspond to facets, some of them indicated by arrows. (b) Typical topographic STM image ($V_s = +2.0$ V, I_t = 0.2 nA) of a facet surface. Numerous protrusions ascribed to facets with a size of a few nm were observed.

According to STM images, many hillocks (a few tens of nm in diameter and a few nm in height) appeared on the surface, as shown in Fig. 11(c). Although the shapes of the facet islands were not clear in the STM images, these hillocks should be the origin of the facet patterns in the LEED and RHEED patterns. From the results of XPS, we found that the facet surface was Ga-rich, corresponding to the higher desorption of NH_3 than Ga and GaCl below approximately 600°C in TPD (Fig. 4). At present, although the mechanism of facet formation by annealing in UHV is not clear, facets are thought to grow mainly by the sublimation of nitrogen; the enhancement of grooves on the surfaces in the sublimation produces isolated 3D islands with facets. Instead of GaN facets, the segregated Ga droplets was also suggested. Anyway, the stoichiometry is broken on the faceting rough surfaces, and these unbalanced rough surfaces could not be recovered by additional treatments.

4.2 Sputtering

Ar ion sputtering is commonly used to prepare clean surfaces and has been used for Ga compound III-V semiconductor surfaces such as GaP, GaAs, GaSb, and GaN. For GaN, it was reported that nitrogen ions are more effective than Ar and Xe ions in removing C and O, and subsequently the annealed surfaces exhibited greater ordering. In previous studies, the reduction of surface contamination and the appearance of 1×1 surface diffraction patterns were revealed. Here, we present the surface structures and compositions obtained through Ar^+ sputtering and subsequent annealing, and discuss their microscopic phenomena. We found that Ar^+ sputtering of the GaN surface is very effective for removing oxide and carbide from the surface, but the enhancement of surface roughness caused by the sputtering could not be recovered by postannealing.

The as-received GaN surfaces have carbon and oxygen as impurities (Table 1 and Fig. 8(b)). Ar ion sputtering is effective for removing C and O surface contamination. Table 1 and Fig. 12(a) show a significant reduction of C 1s, O 1s, and Ga 3d (Ga_{O_x}) components with increasing sputtering time. After 20 min Ar^+ sputtering, the C 1s peak was not detectable and the surface oxygen component was only a few atomic%. As previously mentioned, HVPE GaN (HVPE1 and HVPE2) samples include Cl as an impurity. In XPS spectra, small but obvious Cl 2s, 2p, and Auger peaks (<1 atomic%) always appeared, even after Ar^+ sputtering. This implies the existence of Cl in the bulk of the HVPE HVPE1 samples, as mentioned in subsection 3.3. Figure 12(a) shows a higher rate of increase of Ga 3d (Ga_N) than that of N 1s (N_{Ga}) with increasing sputtering time; the intensity of Ga_N increases over tenfold while that of N_{Ga} increases around threefold after 20 min sputtering. The Ga_N and N_{Ga} intensities against all elements observed on the surface increased from 16 to 26 atomic% and 15 to 22 atomic%, respectively, as shown in Table 1. The higher rate of increase of Ga_N is thought to be caused by the difference in sputtering efficiency between Ga and N. A molecular dynamics simulation showed that Ga atoms are always sputtered with N atoms in pairs, while N atoms are mostly sputtered alone. This simulation also showed that in Ar^+ sputtering at an incident energy of 500 eV, the nitrogen sputtering yield is about five times higher than that of gallium. This indicates that the Ar^+-sputtered GaN surface does not maintain its stoichiometry and becomes Ga-rich at the near-surface. Under our conditions (20 min sputtering), however, the stoichiometry did not change greatly (Table 1), despite the increase of the Ga_{H-N} and N_{H_2} components. The hydrogen included in the samples is expected to play a role in stabilizing the stoichiometry against sputtering.

Figure 12(b) shows a typical RHEED pattern of an HVPE1 sample after Ar^+ sputtering for 20 min and subsequent three-step annealing (200°C for 12 hrs. + 400°C for 1 hr. + 500°C for 5 min). Compared with Fig. 9(c), the 1×1 spots are more diffused and the background level is higher. Faint transmission spots (cyan circles) are seen. The transmission spots indicate the existence of three-dimensional (3D) islands on the surface. Indeed, we observed many islands in STM images as shown in Fig. 12(c). In the RHEED patterns some faint transmission diffraction patterns and chevron patterns corresponding to facets were also observed at different incident azimuth angles. The chevron patterns, implying the presence of facets, were observed after 600°C annealing for both 10 min and 12 hrs. The existence of epitaxial 3D GaN islands implies that the recovery from an Ar^+-sputtered surface is not sufficient to form a flat surface; postannealing cannot produce a flat surface. In contrast, without Ar^+

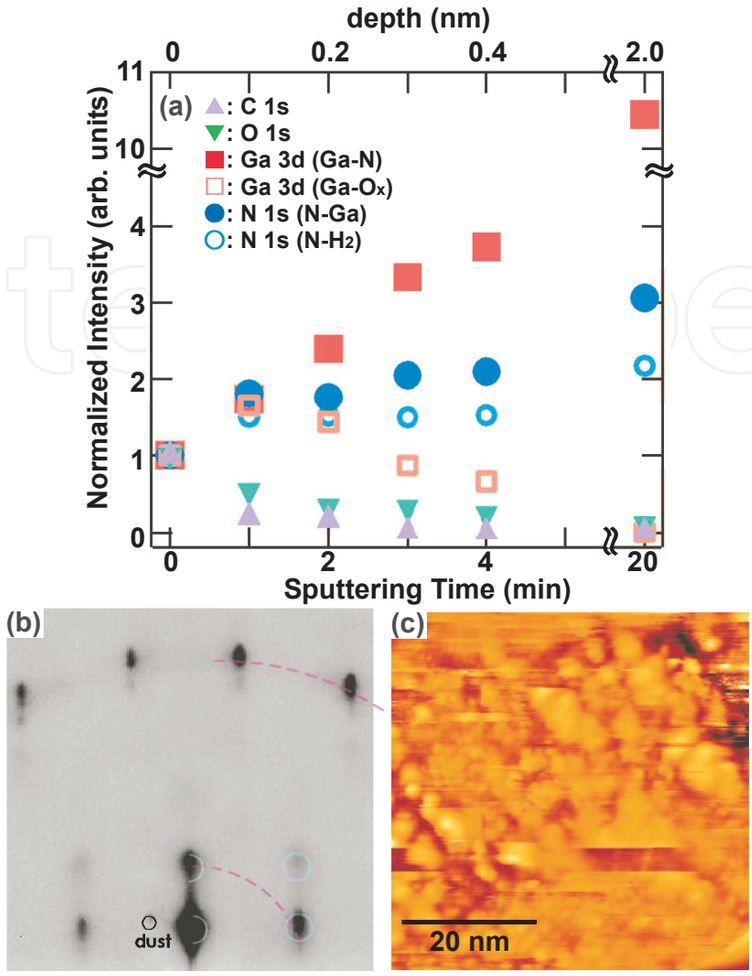

Fig. 12. (a) Normalized XPS intensities of components of C 1s (purple triangles), O 1s (green inverted triangles), Ga $3d_{(Ga_N)}$ (red solid squares), Ga $3d_{(GaO_x)}$ (pink open squares), N $1s_{(N_{Ga})}$ (blue solid circles), and N $1s_{(N_{H_2})}$ (cyan open circles) as functions of Ar^+ sputtering time for HVPE1 samples. Here, each intensity was normalized to the as-received (no-treated) value. The Ar^+ sputtering rate was ~0.1 nm/min. (b) RHEED pattern and (c) STM image for HVPE1 sample after Ar^+ sputtering and subsequent three-step annealing (200°C for 12 hrs., 400°C for 1 hr. and 500°C for 10 min). The incident electron direction was $[1\bar{1}00]$.

sputtering, the intensity of the transmission spots is strong, indicating a large number of epitaxial islands. For HVPE surfaces without Ar^+ sputtering, 3D islands with facets were also formed by annealing above 550 and 600°C. For Ar^+-sputtered HVPE1 samples, the formation of 3D islands started at a slightly lower annealing temperature (500°C). This would imply that the sputtering-induced surface damage leads to easier NH_3 sublimation, thus producing 3D islands. Metallic Ga (α, β, γ, δ, ϵ-Ga, Ga(II), or Ga(III)) in the liquid phase shows halo patterns in diffraction patterns, however, we could not observe any halo patterns in RHEED patterns. According to the STM observation, many small clusters and grains appeared to form.

4.3 Wet treatment

As another surface cleaning approach, we expect chemical etching with subsequent annealing to be also a possible method of obtaining clean and well-defined surfaces. For instance, for Si surfaces chemically etched by a wet process, we can obtain clean surfaces without oxide layers but with hydrogen termination. In general, GaN is chemically stable and expected to be hardly etched (Pankove & Moustukas., 1999). However, GaN can be etched in various chemicals because of the low crystallinity of current GaN crystals. Thus, it is necessary to appropriately control the etching conditions so that oxide layers on the surface are removed while avoiding the erosion of bulk GaN. The GaN surface morphology and stoichiometry depend on the different reactivity between GaN and Ga oxide in different etchants. Therefore, we should predict the reaction in solutions on the basis of a potential-pH equilibrium diagram.

A potential-pH equilibrium diagram, which maps out possible stable phases of an aqueous electrochemical system for a particular metal, can be used as a guide to explain the oxidation and etching reactions of target materials. Although it indicates the condition of Ga metal in solution, it can help us to speculate on the behavior of Ga ions (atoms) in solid GaN bulk in a solution with a certain pH and oxide-reduction potential (ORP). Figure 13 shows a simplified potential-pH equilibrium diagram for the gallium-water system at 25°C (Pourbaix, 1974) showing the four etchant conditions. Figure 13(a) indicates regions of "immunity", "corrosion", and "passivation", depending on the pH and OPR of the solution. The diagram indicates the stability of Ga metal in a specific environment. Immunity shows that the Ga metal has not reacted, while corrosion shows that a general oxidation-reduction reaction occurs and uncharged Ga atoms convert to Ga^{3+} or GaO_3^{3-} ions. Passivation occurs when the metal forms a highly stable coating of Ga_2O_3 on the surface. This theoretical pH-potential diagram is valid under the defined condition, under which no other reactions of Ga^{3+} and GaO_3^{3-} ions, or Ga_2O_3 with other ions occur in the solutions (Pourbaix, 1974). Indeed, for example, Ga_2O_3 dissolves into a solution at all values of pH, as shown in Fig. 13(b). Note that the pH-potential diagram is only valid when the dissolution of all substances is excluded. Thus, when the Ga atoms (ions) of a GaN crystal come in contact with a solution they react to form Ga^{3+}, GaO_3^{3-}, or Ga_2O_3, depending the pH and OPR conditions of the solution, as shown in Fig. 13(a). To obtain an oxide-free balanced-stoichiometry GaN surface, the reaction in the solution should stop before GaN itself starts to be etched by controlling the dipping time.

The solubility of Ga_2O_3 depends on the pH of the solution (Pourbaix, 1974), as shown in Fig. 13(b); the solubility of Ga_2O_3 increases in stronger acidic and basic solutions, that is, at a lower pH and higher pH, respectively. The diagram of Fig. 13(a) predicts the passivation phase, i.e., a Ga_2O_3 coating on a GaN surface, in HF solution, and Fig. 13(b) indicates the etching of Ga_2O_3 in HF solution. Since the reaction speed of the etching is faster than that of the oxidation (Pourbaix, 1974), the rate-determining factor is the oxidation in this case.

The appropriate dipping time in each solution was determined experimentally. Figure 14(a) shows the LEED intensities of the (10) spot (filled circles) as a function of dipping time in 0.5 wt% HF solution for HVPE1 samples without annealing. The figure indicates that dipping for 100 s led to the strongest intensity. The surface stoichiometry was almost retained after 100 s-HF treatment (Ga/N $\sim$0.93 $\rightarrow\sim$0.87), while the surface became considerably Ga-defective/N-rich (Ga/N $\sim$0.64) after 500 s-HF etching. Regarding the roughness obtained

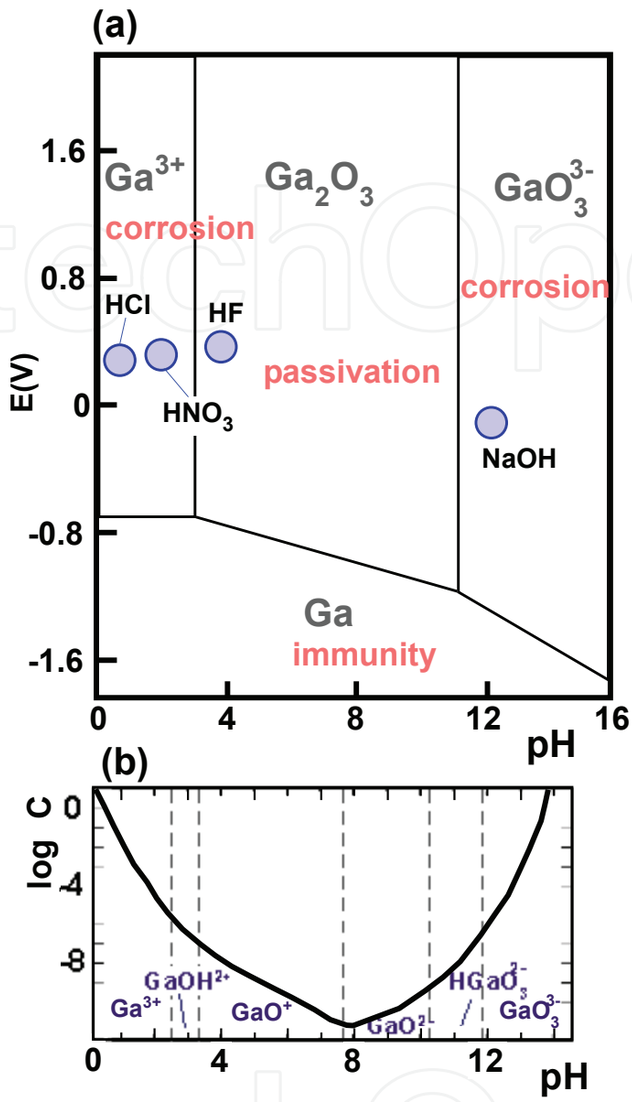

Fig. 13. (a) Potential-pH equilibrium diagram for the gallium-water system at 25°C, quoted from Ref. (Pourbaix, 1974). Predominant ion boundaries are represented by lines. The diagram represents the theoretical conditions (regions) of the "corrosion", "immunity", and "passivation" of gallium. The diagram indicates the stability of Ga metal in a specific environment. Immunity shows that the metal has not reacted, while corrosion shows that a general oxidation-reduction reaction occurs and uncharged Ga atoms convert to Ga^{3+} or GaO_3^{3-} ions. Passivation occurs when the metal forms a highly stable coating of Ga_2O_3 on the surface. The circles represent etchant conditions in this study. (b) Dependence of solubility of Ga_2O_3 on pH in the theoretical equilibrium condition (Pourbaix, 1974). C is the concentration of gallium in solution in all its dissolved forms (g-at Ga/l). The gallium, oxide, and hydroxide ions represented at the bottom are the possible dissolved substances at the pH ranges partitioned by the solid lines.

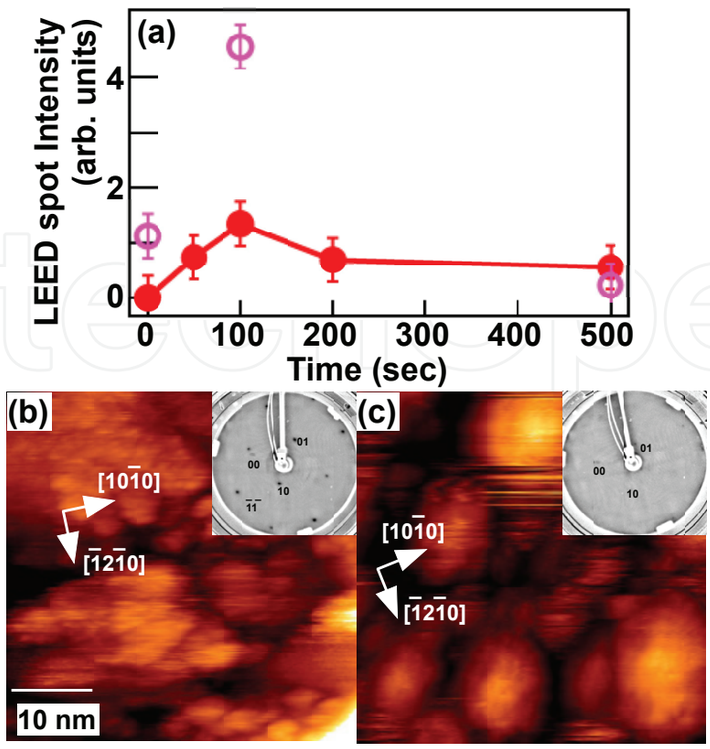

Fig. 14. (a) LEED intensities of the fundamental (10) spot as a function of the HF dipping time for HVPE-GaN samples. Solid circles represent as-treated samples, while open ones represent three-step postannealed samples after the wet treatment. STM images of HVPE-GaN samples dipped in HF for (b) 100 s and (c) 500 s, which were subsequently degassed at 200°C for 12 hrs. in UHV. The LEED condition was E_p = 95 eV in (a)-(c). The STM conditions were (b) $V_s = +4.2$ V, I_t = 0.5 nA and (c) $V_s = -2.8$ V, I_t = 0.5 nA.

from STM, the surface treated with HF for 100 s after degassing had a PV value of ≈ 1.8 nm and an RMS value of ≈ 0.51 nm, making it flatter than an as-received surface (PV ≈ 2.5 nm and RMS ≈ 0.86 nm)(Fig. 14(b)). Reconstructed GaN(0001)2×2 surfaces (GaN(0001)2×2-N) appear on the 100 s-HF treated GaN surfaces by three-step annealing. As shown in Fig. 15(b), the STM image revealed that the surface was very flat with certain atomic defects (PV and RMS were 0.86 and 0.17 nm, respectively). The stoichiometry was almost retained, but, there was a tendency of slightly a Ga-defective/N-rich surface. The surface containing local Ga-defective/N-rich area may explain the formation of GaN(0001)2×2-N on part of the surface after postannealing.

Appropriate etching conditions can lead to clean and reconstructed GaN surfaces. However, inappropriate etching conditions result in rough surfaces with unbalanced stoichiometry. When the dipping time in HF solution exceeded 100 s, many protrusions of ∼10 nm diameter and a few nm in height appeared on the surface, as shown in Fig. 14(c). The surface flatness and stoichiometry could not be recovered by any treatment. This result means that Ga atoms in the solid GaN crystal are oxidized to Ga_2O_3 and subsequently dissolve, assuming the inert property of the paired N atoms, resulting in a rough surface with unbalanced stoichiometry (N-rich/Ga-defective) when the dipping time exceeds 100 s.

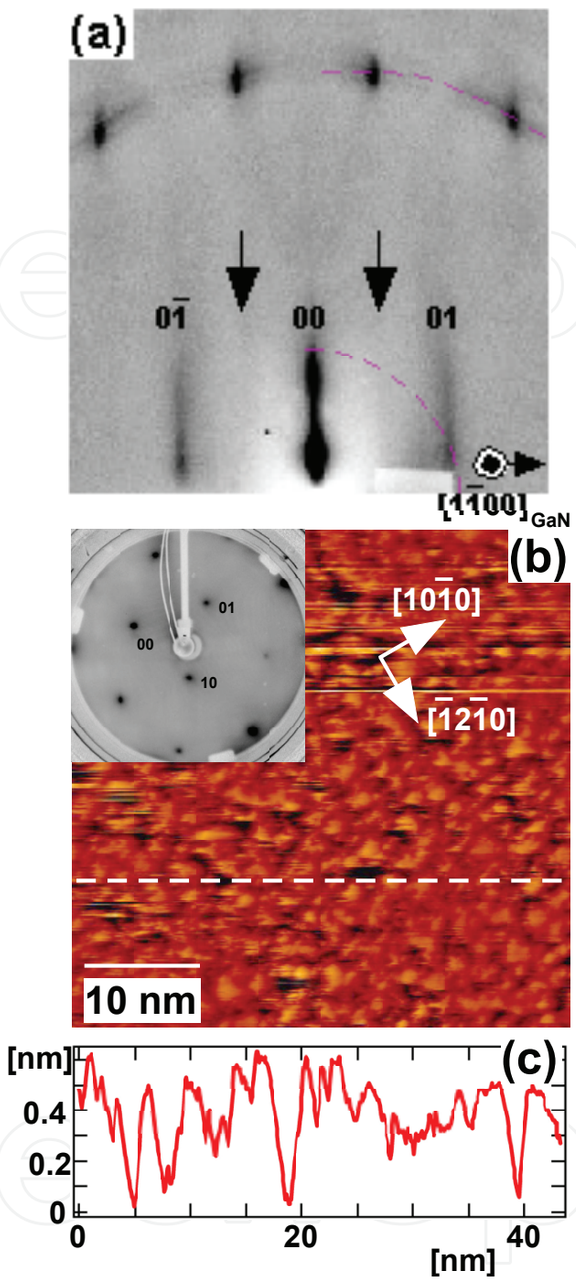

Fig. 15. (a) RHEED pattern, (b) STM images with inset of LEED image for HVPE1-GaN samples after 100 s-HF treatment and three-step postannealing in UHV. In the RHEED patterns, faint 2×2 surface reconstruction streaks (indicated by arrows) can be seen, in addition to 1×1 surface streaks on the integral Laue zones (L_0 and L_1). (c) Cross-sectional profile through the dashed lines in (b). PV and RMS were 0.86 and 0.17 nm. The incident electron energies for RHEED and LEED were 15 keV and 95 eV, respectively. The STM condition were $V_s = -2.5$ V, I_t = 0.5 nA.

In the case of HCl, HNO_3, and NaOH solutions which are in the "corrosion" region, the etching treatment led to an oxide-free surface, but unbalanced Ga-defective/N-rich stoichiometry (Table 1), even for appropriate etching time (Hattori et al., 2010). The pH-E diagram of Fig. 13(a) predicts Ga elution as Ga^{3+} or GaO_3^{3-} in the corrosion phases in HCl, HNO_3, and NaOH solutions. The unbalanced Ga-defective/N-rich stoichiometry after etching means in addition to Ga_2O_3 etching, Ga elusion on GaN surface was occurred. STM images after postannealing revealed that the HNO_3 (HCl)-treated sample had a rough surface and the NaOH-treated sample had many small protrusions. The different types of corrosion may induce different morphologies: huge protrusions are formed by HNO_3 and HCl and small protrusions by NaOH (Figs. 16(a) and (b)). For the surface cleaning procedures of GaAs and GaP, only HF solution produced oxide-free and stoichiometry-balanced surfaces, while HCl solution created an As-rich GaAs(001) surface.

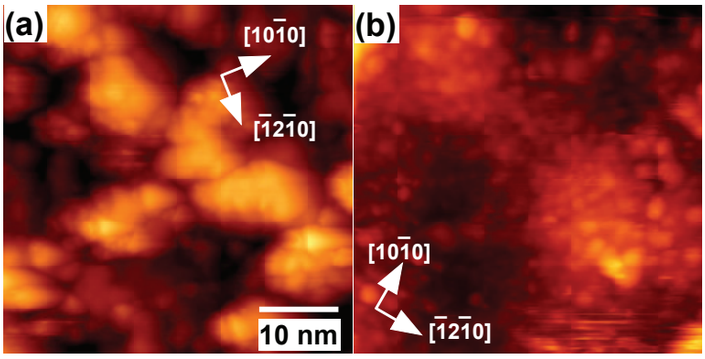

Fig. 16. Typical STM images after three-step annealing of (a) HNO_3- and (b) NaOH-treated HVPE-GaN samples. The STM image of a HCl-treated and postannealed surface was similar to that (a). The STM conditions were (a) $V_s = -4.5$ V, I_t = 0.3 nA and (b) $V_s = +4.5$ V, I_t = 0.4 nA.

The important points for wet treatment are to select suitable etchant solutions whose pH and ORP are in the "passivation" region and to control the etching time in those solutions. At the first trial, lower concentration solutions should be used because it is easier to control the reactions.

5. Summary

We summarize the surface structures, morphology, and stoichiometry of GaN(0001) surfaces treated by annealing in UHV, sputtering, and chemical solutions. For the UHV-treated GaN surfaces, there were structure differences among samples under the same treatment, and we clarified the effect of crystal quality, such as dislocations, the concentration of hydrogen impurities, and the residual reactant molecules in GaN films, on the surface structure. Because of hydrogen impurities, nitrogen desorbs as ammonia upon annealing above a temperature of 600°C, and the clean surfaces with balanced stoichiometry could not be produced. The sputtering treatment was effective in removing C and O surface contamination, but the increased surface roughness as a result of Ar^+ sputtering could not be recovered by postannealing, and the formation of 3D islands with facets was enhanced on the sputtered surfaces. Because the nitrogen sputtering yield is about five times higher than that of gallium,

the Ar^+-sputtered GaN surface does not maintain its stoichiometry and becomes Ga-rich at the near-surface. In the case of performing wet etching on a GaN system, selecting an etchant solution with a certain pH and oxide-reduction potential and controlling the etching time are important to obtain an oxide-free and balanced-stoichiometry surface.

For GaN(0001) surfaces, an unbalanced surface stoichiometry typically leads to a very rough Ga-rich surfaces(Figs 11(b), 12(c), 16(a), and 16(b)) or N-rich surfaces ((Figs 11(d) and 14(c)). For the binary compound GaN system, Ga and N have different reactions to annealing, sputtering (gas reaction), and wet etching (wet chemical reaction, and the stoichiometry is easily broken. The surface morphology showed close correlation with the surface stoichiometry. The structures of clean and flat surfaces are of particular importance since knowledge of the structures is the first step in understanding the fundamental issues of contact formation, chemical reactivity, growth processes, and so on. To obtain clean and flat GaN(0001) surfaces, we should understand the reaction differences between Ga and N, and maintain their stoichiometry.

6. Acknowledgements

The authors acknowledge helpful discussions with Prof. Hiroshi Daimon and Prof. Ken Hattori. ANH also expresses many thanks to her beloved husband Ken for useful advices and constant encouragement throughout this investigation.

7. References

Hattori A. N., Endo K., Hattori K. & Daimon H. (2009) GaN(0001) surfaces on commercial hydride vapor phase epitaxy and metal-organic chemical vapor deposition substrates in ultra high vacuum *Applied Surface Science*, Vol. 256, pp 4745-4756.

Hattori A. N., Kawamura F., Yoshimura M., Kitaoka Y., Mori Y., Hattori K., Daimon H. & Endo K. (2010) Chemical etchant dependence of surface structure and morphology on GaN(0001) substrates *Surface Science*, Vol. 604, pp 1247-1253.

Properties of Group III Nitrides, edited by Edgar J. H.(1994) INSPEC, London.

Strite S. & Morkoc H. (1992) GaN, AlN, and InN: A review *Journal of Vacuum Science and Technology B*, Vol. 10, pp 1237-1266.

Waltereit P.,Brandt O. , Trampert A., Grahn H. T., Menniger J., Ramsteiner M., Reiche M., & Ploog K. H. (2000) Nitride semiconductors free of electrostatic fields for efficient white light-emitting diodes *Nature*, Vol. 406, pp 865-868.

Maruska H. P. & Tietjen J. J. (1969) The preparation and properties of vapor-deposited single-crystal-line GaN *Applied Physics Letter* Vol. 15, pp 327-329.

Hydrogen in Semiconductors II, Nickel N. H. (1999) Academic Press, Berlin.

Amano H., Sawaki N., Akasaki I., $ Toyoda Y. (1986) Metalorganic vapor phase epitaxial growth of a high quality GaN film using an AlN buffer layer *Applied Physics Letters* Vol. 48, pp 353-355.

Reflection High Energy Electron Diffraction, Ichimiya A. & Cohen P. I. (2004) Cambridge University Press, Cambridge.

Murata J., Sadakuni S., Yagi K., Sano Y., Okamoto T., Arima K., Hattori ĄA. N., Mimura H. & Yamauchi K. (2009) Planarization of GaN(0001) Surfaces by Photo-Electrochemical

Method with Solid Acidic or Basic Catalyst *Japanese Journal of Applied Physics*, Vol. 48, pp 121001-1-4.

Feenstra R. M., Chen H., Ramachandran V., Smith A. R. & Greve D. W. (2000) Reconstructions of GaN and InGaN surfaces *Applied Surface Science*, Vol. 166, pp165-172.

Gallium Nitride Pankove J. I. & Moustukas T. D. (1999) Academic Press, San Diego.

Atlas of Electrochemical Equibilia in Solutions Pourbaix M. (1974) NACE, Houston.

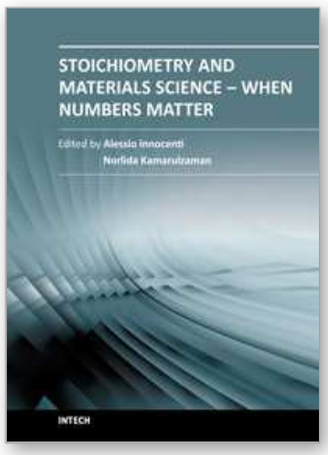

Stoichiometry and Materials Science - When Numbers Matter

Edited by Dr. Alessio Innocenti

ISBN 978-953-51-0512-1
Hard cover, 436 pages
Publisher InTech
Published online 11, April, 2012
Published in print edition April, 2012

The aim of this book is to provide an overview on the importance of stoichiometry in the materials science field. It presents a collection of selected research articles and reviews providing up-to-date information related to stoichiometry at various levels. Being materials science an interdisciplinary area, the book has been divided in multiple sections, each for a specific field of applications. The first two sections introduce the role of stoichiometry in nanotechnology and defect chemistry, providing examples of state-of-the-art technologies. Section three and four are focused on intermetallic compounds and metal oxides. Section five describes the importance of stoichiometry in electrochemical applications. In section six new strategies for solid phase synthesis are reported, while a cross sectional approach to the influence of stoichiometry in energy production is the topic of the last section. Though specifically addressed to readers with a background in physical science, I believe this book will be of interest to researchers working in materials science, engineering and technology.

InTech Europe
University Campus STeP Ri
Slavka Krautzeka 83/A
51000 Rijeka, Croatia
Phone: +385 (51) 770 447
Fax: +385 (51) 686 166
www.intechopen.com

InTech China
Unit 405, Office Block, Hotel Equatorial Shanghai
No.65, Yan An Road (West), Shanghai, 200040, China
中国上海市延安西路65号上海国际贵都大饭店办公楼405单元
Phone: +86-21-62489820
Fax: +86-21-62489821

IntechOpen